Verifiable Smart Packaging with Passive RFID

Ge Wang, *Member, IEEE*, Jinsong Han, *Senior Member, IEEE*, Chen Qian, *Member, IEEE*, Wei Xi, *Member, IEEE*, Han Ding, *Member, IEEE*, Zhiping Jiang, *Member, IEEE*, and Jizhong Zhao, *Member, IEEE*

Abstract—Smart packaging adds sensing abilities to traditional packages. This paper investigates the possibility of using RF signals to test the internal status of packages and detect abnormal internal changes. Towards this goal, we design and implement a nondestructive package testing and verification system using commodity passive RFID systems, called Echoscope. Echoscope extracts unique features from the backscatter signals penetrating the internal space of a package and compares them with the previously collected features during the check-in phase. The use of backscatter signals guarantees that there is no difference in RF sources and the features reflecting the internal status will not be affected. Compared to other nondestructive testing methods such as X-ray and ultrasound, Echoscope is much cheaper and provides ubiquitous usage. Our experiments in practical environments show that Echoscope can achieve very high accuracy and is very sensitive to various types abnormal changes.

Index Terms—RFID, package identification

1 Introduction

Identifying and tracking items are crucial tasks for various automatic management systems with applications of logistics, supply chain, and retailing. Towards this purpose, Radio Frequency Identification (RFID) systems have been developed and widely utilized. An RFID tag attached to the surface of an item serves as the label to identify the item and can be recognized by an RFID reader. RFID-based smart packaging systems have been proposed. However, the essential mechanism of RFID-based smart packaging is to identify the tags rather than the items inside packages. Consider these cases in an RFID-based logistic system. An intruder may steal the items in a tagged package or replace the expensive items by cheap ones. A terrorist may add bombs to an ordinary baggage during transportation. RFID systems have no ability to detect such malicious behaviors that change the internal status of tagged packages.[1] Hence testing and verifying the internal status of packages is of importance for the authenticity, integrity, and safety of automatic management systems. In this paper, we target on the problem of verifying the internal status of packages and detecting abnormal changes of the internal items.

1. Hereafter we use "package" to refer to any types of containers.

- *G. Wang, W. Xi, H. Ding, and J. Zhao are with the Department of Computer Science and Engineering, Xi'an Jiaotong University, Shaanxi 710049, China. E-mail: wangge@stu.xjtu.edu.cn, {xiwei, dinghan, zjzj}@mail.xjtu.edu.cn.*
- *J. Han is with Zhejiang University, Hangzhou 310027, China. E-mail: hanjinsong@gmail.com.*
- *C. Qian is with the Department of Computer Engineering, University of California Santa Cruz, Santa Cruz, CA 95064. E-mail: cqian12@ucsc.edu.*
- *Z. Jiang with the Institute of Software Engineering School of Software, Xidian University, Shaanxi 710126, China. E-mail: flyinfeeling@gmail.com.*

Manuscript received 5 Apr. 2017, revised 25 Mar. 2018, accepted 19 June 2018, Date of publication 3 July 2018; date of current version 1 Apr. 2019.
Corresponding author: Ge Wang.
For information on obtaining reprints of this article, please send e-mail to: reprints@ieee.org, and reference the Digital Object Identifier below.
Digital Object Identifier no. 10.1109/TMC.2018.2852637

Obviously physical inspection that requires opening the packages is slow and labor-intensive. Instead, nondestructive testing that evaluates the packages without causing any physical changes to them is more preferred. However, prior solutions for nondestructive testing is not suitable for testing the internal status and changes of containers. Among them, x-ray screening, ultrasonic testing, seal tag and weighting are four typical non-destructive approaches for package identification. However, these methods are all not suitable for package identification. Some of them are designed for different purposes (X-raying and ultrasonic testing). Some of them need extra expensive devices (X-raying and ultrasonic testing). And some of them verify the package characteristics rather than the inner objects (seal tag and weighting). We specify their drawbacks in Section 6.1.

To our knowledge, no existing work has successfully used RF signals for internal status checking and verification of a package. In this work we investigate the possibility of RF-based low-cost and nondestructive testing. The key idea of RF-based nondestructive testing is to extract distinct features from the signal penetrating the internal space of a package. However, using RF signals to identify the internal structure like X-rays is difficult. Different from X-rays, RF wavelengths are too long to delicately depict the shapes of the items inside the package, and the different absorption rates for different materials using RF signals can hardly be recognized. RF-based testing cannot produce images like those in X-ray screening.

In our application scenarios, an automatic management system always has a check-in site where the identifier (such as the barcode or the tag ID) and other features of a package can be collected and stored in a database. Then at another testing site, different from the check-in site, the testing system should be able to verify whether the internal status inside the package has been changed. *We assume packages are tightly filled and packed*. Hence items can hardly be relocated inside a package.

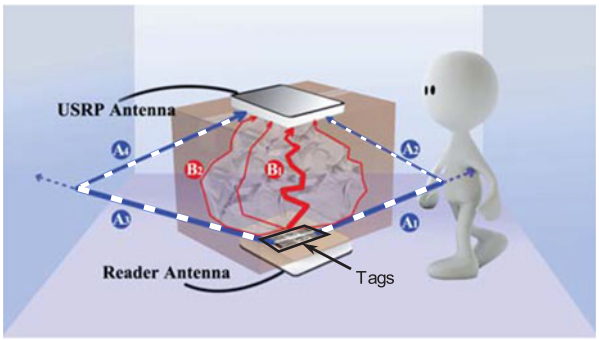

Fig. 1. Overview of Echoscope.

Since at a testing site we only require to *verify* whether the internal status of a package is changed, the testing system does not need to identify the shapes and material of the items in a package. It only needs to determine whether the ID and signal features collected at a testing site match the original record. However, directly using the power of RF signals sent from a normal transmitter (such as WiFi) for nondestructive testing is still impractical, because the differences among radio sources and environments at different sites may cause different RF signal features and result in false acceptance or false rejection in testing results.

To resolve these challenges, we propose to utilize *backscatter communication* of passive RFID systems as the RF source for nondestructive testing. The proposed system Echoscope is built using commodity off-the-shelf (COTS) RFID readers and tags. The structure of Echoscope is shown in Fig. 1. For each package, we paste *a pair of tags* in parallel at the center of its inner-bottom side. At the check-in and testing sites, the package is placed on top of an RFID reader. In addition we deploy a monitor with a Universal Software Radio Peripheral (USRP) model N210 at the top of the package to collect the RF signals from the reader and tags. At the check-in site, for each package Echoscope collects the RF signals of backscatter communication between the tags and reader and stores them in a database. At a different testing site, Echoscope repeats the signal collection step and compares the extracted features with the record in the database.

We have implemented prototype systems of Echoscope and conducted extensive experiments. The evaluation results in various environments show that Echoscope exhibits a high accuracy in detecting abnormal changes for a large variety of items. The false accept rate of Echoscope using three types of RFID tags is as low as 4.76 percent in average.

The remaining paper is organized as follows. We present the system model in Section 2 and the detailed design in Section 3. In Section 4, we propose an advanced version of Echoscope, i.e., MPT. In Section 5 we describe the implementation of Echoscope and show the experiment results. We introduce the related work in Section 7. In the end we conclude this work in Section 8.

2 Basic Idea and Experimental Validation

In this section, we present the basic idea of Echoscope to extract features from backscatter signals.

2.1 Backscatter Communication

According to the EPC C1G2 protocol [1], an RFID reader identifies passive tags following the procedure outlined in Fig. 2.

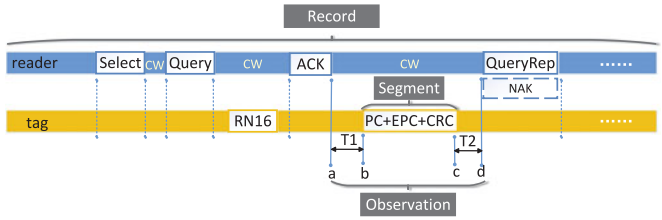

Fig. 2. EPC C1G2 protocol.

We find that only when the reader acknowledges the tag with an invalid *ACK* that contains the correct *RN16*, the tag will backscatter its identifier code (*ID*) (including the Protocol-Control *PC*, Electronic Product Code *EPC*, and Cyclic Redundancy Check *CRC*). Upon receiving the *ID* successfully, the reader sends *QueryRep*/*Query*/*QueryAdjust* to start a new time slot. In our system design, we only utilize the *ID* segments of tags as the feature sources, the details are specified in Section 2.2.

2.2 Feature Source Selection

A sequence of radio signal received by the monitor of Echoscope includes three components: basic signal from the radio source, noise caused by environmental factors, and signal changes caused by the propagation medium in the packet internal space. The essential goal of Echoscope is to extract the feature of RF signals penetrating the internal space while eliminating the environmental noise. We choose to extract features from tag backscatter signals. This approach matches well to the requirements of Echoscope due to the following considerations. First, the tags attached to the package are consistent signal sources at different sites. Hence signal changes introduced by differences among devices are minimized in the feature extraction process. We only need to eliminate environmental noise. Second, tag will always respond the same data (tag's ID) when it is queried. This property ensures that whenever and wherever we test the package, the tags can provide consistent signals from the sources. Although these signals may still be different due to the difference among the packet internal space and the environment of the testing sites, we may use advanced strategies to extract the features that are caused by the packet internal status only. We will introduce how we eliminate environmental noise in the next subsection.

2.3 Reduction of Environmental Noise

When the signal sources are identical, the next step is to eliminate or reduce the environmental noise. Our important design choice is to use *a pair of tags* instead of a single one to eliminate the noise and extract the packet internal feature. In this section, we first propose a theoretical model showing how we use a pair of tags to reduce noise and then we demonstrate our experimental results that validate the proposed model.

As shown in Fig. 1, the signal backscattered from a tag mainly experiences three propagation effects, *i.e.*, reflection, diffraction, and refraction, before it reaches the monitor antenna. We decompose a backscatter signal received by the monitor into two categories, namely the *characteristic* and *noisy* parts. As shown in Fig. 1, the characteristic part, marked in red color(line $B1 \sim B2$), convey the features of

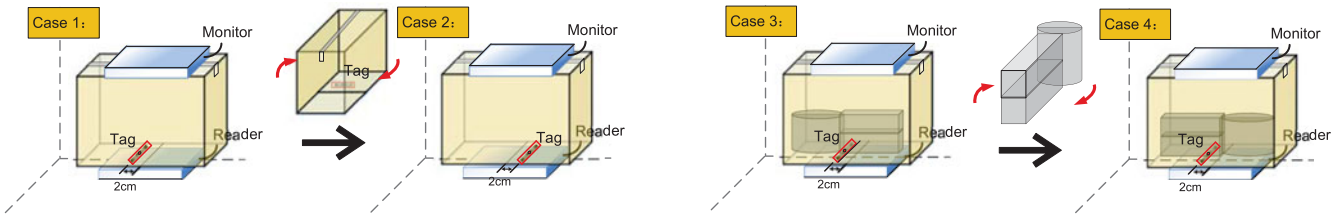

(a) Experiment 1 (b) Experiment 2

Fig. 3. Two sets of experiments to validate $F - F' \gg N_{en} - N'_{en}$.

the internal status of the package. They mainly comprise of the refracted and diffracted signal by the inside items and package. The noisy part, marked in blue color(line $A1 \sim A4$), do not provide any feature information about the package. They are mainly reflected by the environment. Hence Echoscope needs to extract features from the characteristic signal. However, it is challenging to eliminate noisy signal by reading only a single tag.

We propose to solve this problem by placing two tags at the inner-bottom side of each package. We use F and N_{en} to represent the characteristic and noisy parts of the signal respectively. Given two tags, tag 1 and tag 2, in a package, the received signals at the monitor, denoted as S_1 and S_2, can be represented as follows.

$$\begin{aligned} S_1 &= ID_1 + T_1 + F_1 + N_{en} + N_{eq} + N_w \\ S_2 &= ID_2 + T_2 + F_2 + N'_{en} + N'_{eq} + N'_w. \end{aligned} \tag{1}$$

Here ID_1 and ID_2 are the ID information of both tags, in the sequence $(PC + EPC + CRC)$. T_1 and T_2 are the signal part caused by hardware characteristics of the two tags. N_{eq} and N'_{eq} are the noise introduced by the monitor, and N_w and N'_w are white Gaussian noise.

If we compute the difference between S_1 and S_2, we have:

$$\begin{aligned} S_1 - S_2 =& (ID_1 - ID_2) + (T_1 - T_2) + (F_1 - F_2) \\ &+ (N_{en} - N'_{en}) + (N_{eq} - N'_{eq}) + (N_w - N'_w). \end{aligned} \tag{2}$$

For a given pair of tags, $(ID_1 - ID_2)$ and $(T_1 - T_2)$ are always identical whenever the reader interrogates them. Moreover, the noises introduced by the monitor, denoted as N_{eq} and N'_{eq} for tag 1 and 2, are also similar at a same time. Then we may have:

$$S_1 - S_2 = C + (F_1 - F_2) + (N_{en} - N'_{en}) + (N_w - N'_w), \tag{3}$$

where $C = (ID_1 - ID_2) + (T_1 - T_2)$. Note that two noise signal vectors N_w and N'_w are independent to each other. Similarly, F_1 and N_w are independent, and F_2 and N'_w are also independent. Let $G = N_w - N'_w$. We have $G \sim N(0, \delta_{i'}^2 + \delta_{j_0}^2)$. If Echoscope collects sufficiently many signal samples from both of the two tags, according to the law of large numbers [2], the difference of the sum of $(N_w - N'_w)$ and the expectation of variable G is infinitely close to 0:

$$\lim_{n\to\infty} \sum \left[(N_w - N'_w)\right]/n - E(G) \leq \epsilon. \tag{4}$$

Since $E[G] = 0$, we further have the following equation:

$$E[S_1 - S_2] = C + E[(F_1 - F_2) + (N_{en} - N'_{en})]. \tag{5}$$

Since N_{en} and N'_{en} are introduced by two tags at very close positions, we conjecture that N_{en} is very similar to N'_{en}. It is based on an intuition that the distance between the two tags is much shorter than the distance from them to the objects in the environment. In other words, tags at very close positions may share very similar ambient noises and multipath effects. Prior researches, such as [3] and [4], have demonstrated this fact.

In fact, if we can verify that $F_1 - F_2 \gg N_{en} - N'_{en}$, we can assume that the feature difference $(F_1 - F_2)$ plays a dominant role in the above equation. As a result, $\sum(S_1 - S_2)$ can then be considered as a valid feature source of the internal status of the package. We propose the following conjecture.

Conjecture. Given a certain package tested by Echoscope in a random environment and the two tags are close to each other within a few centimeters. For feature signals F and F' and environmental noise N_{en} and N'_{en}, we have $F_1 - F_2 \gg N_{en} - N'_{en}$.

We use experiments in real environments to verify the above conjecture. In addition, we also obtain this result from detailed theoretical modeling and analysis. Due to the page limit, we only present the experimental results.

We conduct two sets of experiments to estimate $N_{en} - N'_{en}$ and $F_1 - F_2$ respectively. In the first set of experiments, we intend to estimate $N_{en} - N'_{en}$ by eliminating the influence of tag hardware differences C as well as that of feature difference $F_1 - F_2$. The idea of the experiments is to use a same tag to make $C = 0$ and use a completely empty package to make $F_1 = F_2$. As shown in Fig. 3a, we first attach the tag to the inner-bottom side of the package with 2 cm distance to the center and let the monitor collect 800 signal samples. Then we rotate the package for 180 degrees and make the tag on the other side, still with 2 cm distance to the center. The monitor collects another 800 signal samples. The two sets of signal samples can be used to simulate a pair of identical tags with 4 cm distance to each other. Since the package is completely empty, we can assume that $\sum(F_1 - F_2) = 0$. Also $C = (ID_1 - ID_2) + (T_1 - T_2) = 0$ for a same tag. Therefore,

$$E[S_1 - S_2] = E[N_{en} - N'_{en}]. \tag{6}$$

We show the two sets signal samples in the top figure of Fig. 4a, as "case 1" and "case 2". Their difference is shown in the bottom one of Fig. 4a. We find that the average amplitude of $S_1 - S_2$ is in the order of 10^{-4}, much smaller compared to the amplitude of S_1 and S_2 in the order of 1.

To estimate $(F_1 - F_2)$, we conduct another set of experiments. As shown in Fig. 3b, we fill the package with some objects and let the monitor collect 800 signal samples. Then we relocate the objects in the package and make them as the mirror images to the original locations. Then the monitor

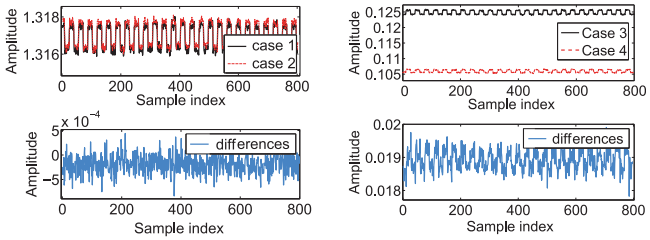

(a) Estimation of $N_{en} - N'_{en}$ (b) Estimation of $F - F'$

Fig. 4. Estimation of $N_{en} - N'_{en}$ and $F - F'$.

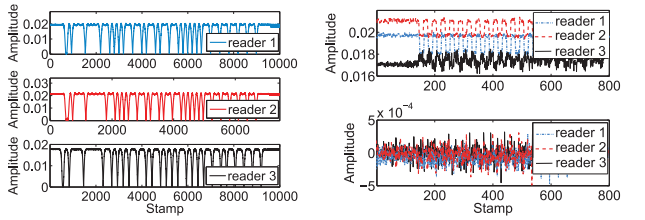

(a) The commands of different readers (b) The tag's signals and the differences between two adjacent tag's signals

Fig. 5. Estimation of $N_{en} - N'_{en}$ and $N_{eq} - N'_{eq}$.

collects another 800 signal samples. In the two experiments, the environment is maintained to be identical. Since the tag does not move in the two experiments, we may consider the environmental noise is very close,*i.e.*, $N_{en} - N'_{en} = 0$. Also $C = 0$. Hence,

$$E[S_1 - S_2] = E[F_1 - F_2]. \tag{7}$$

In Fig. 4a, the top figure shows the signal samples of S_1 and S_2 of the two sets of experiments. We can see that they differ significantly. The bottom figure shows their difference, *i.e.*, $S_1 - S_2$. The average difference, $E[S_1 - S_2] = E[F_1 - F_2]$, is in the order of 10^{-2}. Hence $E[F_1 - F_2]$ is larger than $E[N_{en} - N'_{en}]$ by about two orders of magnitude. We also try different materials to fill the package, including alloy, water, wood, clothes, and carton, and confirm that 10^{-2} is a normal value for $E[F_1 - F_2]$.

Our experiments validate the conjecture that $F_1 - F_2 \gg N_{en} - N'_{en}$, which means the dynamic component of $S_1 - S_2$ is dominated by the features of the package internal status, including the structure, material, and positions of the objects inside the package. In addition, we conduct similar experiments to estimate that the value of C is smaller than 10^{-3}. Due to the space limit, we skip the details.

Conjecture. The equipment noise N_{eq} and environment noise N_{en} in backscattered signals can be eliminated by the aforementioned subtraction method.

The backscattered signals in the RFID system are mostly related to the hardware characteristics of both the reader and tags. Therefore, we aim to discuss whether the equipment noise N_{eq} can be also eliminated by our subtraction. Echoscope leverages the subtraction between the signal segments of two adjacent *ID*s from the two tags to remove the impact of different readers and sites. Hence, the equipment noise N_{eq} mainly derived from the reader and environment noises N_{en} can be effectively eliminated. In addition, we conduct an experiment to verify the feasibility and performance of this subtraction. We use three types of readers, i.e., Impinj R220 (reader 1), Impinj R420(reader 2) and Alien ALR9680(reader 3), to interrogate an Impinj E41C tag in different sites, where we collect the signals backscattered from the tag upon the interrogation from these three readers, respectively.

We plot the results in Fig. 5. Fig. 5a presents the tag's backscattering signal fragments corresponding to its *ID* under the three readers' interrogations. We find that for the interrogation from each individual reader, the signals backscattered from the tag are not identical. Fortunately, the reader's impacts can be effectively eliminated by using the subtraction solution in Echoscope. The consistency of backscattering signals can be proved by the results shown in the lower part of Fig. 5b. In this subfigure, we show the differences between two adjacent signal segments corresponding to the tags' *ID*s, i.e., $S_1 - S_2$. Since the relative position of the tag and two antennas are the same, so we can safely assume that $F_1 - F_2 = 0$. And the characteristic of the tags' signal are all the same to the tag now, we can assume that C = 0. Therefore,

$$E[S_1 - S_2] = E[(N_{eq} - N'_{eq}) + (N_{en} - N'_{en})]. \tag{8}$$

From the result, we find that for the same reader and tag, the difference of two adjacent *ID* signal segments is extremely lower(10^{-4}), which means the equipment noise N_{eq} and environment noise N_{en} can be eliminated by performing Echoscope. Although the backscattered signals vary among different readers, our subtraction method can effectively reduce or even eliminate the difference.

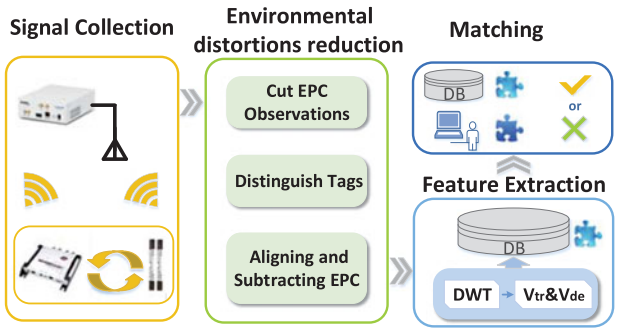

Fig. 6. System workflow.

3 System Design

As shown in Fig. 6, Echoscope comprises four modules, namely *Signal Collection*, *Noise Elimination*, *Feature Extraction*, and *Feature Matching*. In the Signal Collection phase, Echoscope records the raw signals of the backscatter communication from the tags to the reader using the USRP monitor. In the Noise Elimination phase, certain necessary processes are conducted to remove the noise from the raw signals. The Feature Extraction phase extracts features from the backscatter signals. The last module, Feature Matching, decides whether the features from the collected signals match the ones stored in the database.

3.1 Backscatter Signal Collection and Segmentation

We use a *record* to denote the raw signal data recorded by the monitor within a time duration, including all signals sent

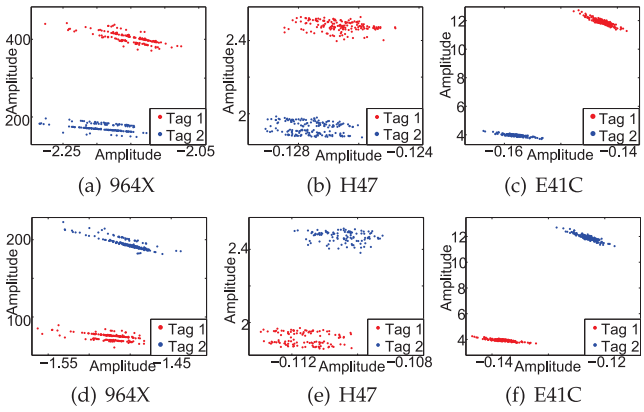

Fig. 7. K-means clustering for observations of two tags after FFT: *(a)(b)(c) show the results of two tags with similar EPCs. (d)(e)(f) show those of two tags with significantly different EPCs.*

from the reader and backscattered from the tags. During this time, the reader keeps querying the two tags and the monitor records the communication signals. The default duration of each record is 1 seconds. Hence a record includes multiple rounds of backscatter communication. Let an *observation* to denote a part of backscatter signals in a record, i.e., the part corresponding to the time duration between the end of an *ACK* and the start of a *QueryRep*. An observation contains the data of the *ID*, *i.e.*, *PC+EPC+CRC*. Echoscope only uses backscatter signals for testing, thus it should filter other RF signal parts.

To achieve this goal, Echoscope needs to identify the observations of a record to obtain the backscatter parts containing the *ID*s by performing accurate *segmentation* on the signal. It is difficult for current commodity readers to perform such operation because the API to analyze signals in detail is not open to public. Instead we utilize USRP N210 as the monitor [5] to record the communication process between the reader and tags. The monitor operates as a passive listener and records the electromagnetic signals.

If the *ID* field of a tag can be directly decoded from the signal captured by the monitor, it would be very easy to segment the signal to get an observation. However, when penetrating the internal space of a package the signals backscattered from tags are distorted and became very difficult to be decoded. Thus, we cannot obtain desired observations directly by decoding. Even if observations are successfully segmented, without ID information Echoscope still cannot identify which tag an observation belongs to. When each record is for 1s time duration, there could be over 100 observations. Hence how to quickly and accurately segment and identify that many observations are another challenge.

We thereby employ an indirect method for extracting observations. This method leverages the reader's signal, which has much higher signal strength than that of a tag. According to the EPC C1G2 specification, a tag replies its *ID* after it receives an *ACK* command from the reader. Then the reader sends another command *QueryRep*. *ACK* and *QueryRep* have preambles of '01' and '00', respectively. By inspecting the signal amplitude from a record and recognizing the preambles of above reader commands, we can find out the edges of desired observations.

We utilize Backscatter link frequency (BLF), which is the frequency of a tag-to-reader link [1], to identify tags based on observations. Due to manufacturing imperfection, BLF determines a tag's responding data rate. It varies among different tags [6] and can be used as a "fingerprint". To extract BLFs from distorted signals, we perform Fast Fourier Transform (FFT) on the observations. We calculate the variance and mean values of the result after FFT, and map them to a two-dimensional plane. Those values can be further clustered in the plane by applying the K-means algorithm. In Fig. 7, we show the results of mapping and clustering about 360 observations monitored from two tags in a package filled with books. We use three types of tags, Alien 964X, Impinj H47, and Impinj E41C. In Fig. 7a, 7b, and 7c, the experiment uses two tags that are with similar EPCs. While in Fig. 7d, 7e, and 7f, the experiment uses two tags with significantly different EPCs. We find that no matter the EPCs are close or not, Echoscope can always separate observations from two different tags. In order to avoid outliers and select the most stable features for each tag, we only choose the top-n candidate observations nearest to each cluster center in the two-dimensional space.

3.2 Environmental Distortions Reduction and Signal Pairing

After the signal collection and segmentation, we can get observations in two groups corresponding to the two tags respectively. From Equation (5), we know that environmental distortions can be reduced by computing the differences of pairs of values from these two groups. However, there are two challenges that are needed to be resolved.

1) Paring temporally adjacent observations. Though we have shown that the environmental noise will not contribute to a dominant factor by performing subtraction on the signals of two tags, we assumed that the pair of signals should be collected at about a same time. Since passive RFID systems usually use random-access algorithms, e.g., the slotted ALOHA protocol, for anti-collision, observations are collected in different time slots. However, external environments may be changed due to the movement of objects, such as a moving person or cart. Selecting observations at very different time slots may fail to eliminate the noise from the external environment. Fortunately, since each time slot is very short (in the order of millisecond), we can expect that two backscattered signals in two close time slots experience the same environmental noise. Therefore, our first effort is to select two temporally adjacent observations for subtraction. Their time slots should be as close to each other as possible. As aforementioned in Section 3.1, in order to avoid outliers and select the most stable features, we only choose the top-n candidate observations for each tag. To pair these observations, we first put them in the order of response time. Then among the $2n$ observations of the two tags, the system selects m pairs, $m < n/2$, each of which includes two observations in two close-by slots.

2) Aligning the starting points of tag responses Another challenge to compute $S_1 - S_2$ for a pair of observations is to align their starting points of IDs. It is necessary because the IDs in different observations start at different time points.

We use the change-point detection (CPD) mechanism to find the start point within each observation. Fig. 8a illustrates an example of locating the start point. The essential idea of CPD is to detect a sharp change in a given curve. Let

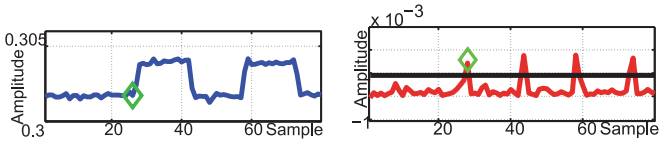

(a) Raw data of EPC (b) Curve of value Δe

Fig. 8. Change point detection.

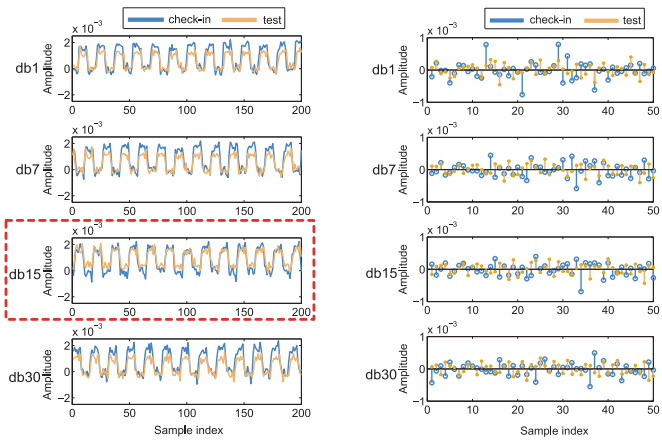

(a) c_a vectors (b) c_d vectors

Fig. 9. c_a and c_d for different Daubechies wavelets.

$EPC(a)$ be the a-th sampling point of the EPC. An intuitive way is to calculate forward difference $\Delta e = |EPC(a+1) - EPC(a)|$, and then check if Δe is higher than a threshold t, which is pre-determined by analyzing existing results. In Fig. 8b, we plot the results of all values of Δe, where the black line is the value of threshold t. The start point, marked by the green square, is accurately located by checking whether $\Delta e > t$.

We arrange all the $(S_1 - S_2)$ results of observation pairs to an $m \times k$ feature matrix F. Here the m is the number of observation pairs and k is the amount of sample points of each EPC.

3.3 Feature Extraction and Matching

After signal pairing, we maintain a feature matrix F, where each row is a vector representing $(S_1 - S_2)$. To extract features that characterize the package internal status, we perform the discrete wavelet transform (DWT) on each row. A discrete signal S can be approximated by a combination of wavelet basis, while the coefficients of this combination can reflect the signal's characteristic. In our applications, the features of items are implied by the tags' responses. The output of DWT is two vectors: the approximation coefficients vector c_a and the detail coefficients vector c_d [7]. To choose an appropriate wavelet basis to analyze the raw data, we conduct two experiments. One is to compare the results of a same object at different locations, e.g., the check-in and test points. The other one is to compare the results using different objects. A good wavelet basis should increase the difference between different objects while shrinking the gap between the same objects. Fig. 9 shows the wavelet basis results from the same objects (alloys) at different locations. The raw data is divided into two vectors, i.e., vector c_a and c_d. The blue curves and points represent results at the check-in site and the orange curves and points represent results at another testing site. db1, db7, db15, and db30 stand for different Daubechies wavelets. By observing large amount of experimental result, we find that the vector c_a of db15 has the best performance than other wavelet basis, because the results from different locations are very close. The system does not need to determine the best wavelet basis every time. The c_d vectors of all the wavelet basis have no obvious similarity for different locations.

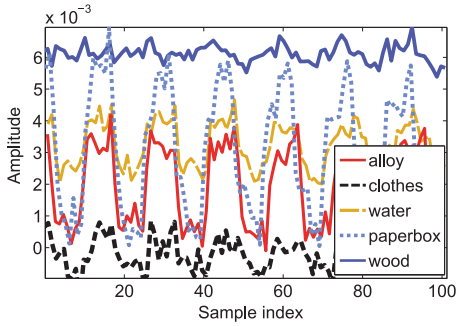

Fig. 10. Vector c_a for different materials

To investigate the performance of db15 in distinguishing different objects, we depict the c_a vectors of db15 with different objects in the package. As shown in Fig. 10, the gap between different materials are obvious and easy to distinguish. Hence, we employ db15 as the wavelet basis in the DWT processing. For each row in the feature matrix F, we use DWT to extract the approximate vector c_a. After this dispose, we have a new matrix D with size $m \times k'$, where m is the number of rows in the feature matrix F and k' is the length after performing DWT. Each row of D is a sequence of coefficient c_a.

By observing the DWT results of different materials in Fig. 10, every material shows very different results in the vector c_a. We tried extracting the coefficient matrix D from the check-in and test results, use them as the train data and testing data respectively, and construct a classifier. However, the classification results are poor (accuracy $< 50\%$). The reason might be that the overall trend of the c_a changes plays a dominate role in classification. However, the details of vector c_a are not reflected in the classifier. Under this consideration, we try to separate the trends V_t and small details V_d of coefficient matrix D. The method is shown as follows.

$$V_t(i) = \frac{\sum_{j=1}^{m} D(j,i)}{m}, 0 < i \leq k'$$
$$V_d(j,i) = D(j,i) - V_t(i), 0 < i \leq k', 0 < j \leq m \quad (9)$$

Then we have a trend vector $V_{t\ 1\times k'}$ and a detail matrix $V_{d\ m\times k'}$. As aforementioned, each row in matrix D represents a sequence of coefficient c_a, which extracts the characteristic from the feature matrix F. The vector V_t reflects the mean level at each corresponding point of rows in matrix D. And matrix V_d keeps a record of the detailed variation at each point of every row. In this way, we can decompose the coefficient matrix D into two parts and compare them respectively.

Identification Logic. We first calculating the cross-correlation coefficient x of vector V_t^c and V_t^t, and compare x with the correlation threshold T. If not satisfied, we set the judgment result R as 0 and consider the package has been attacked. Otherwise, we set $R = 1$ and then utilizing a Naive Bayesian classifier to identify whether V_d^t is the same with

(a) placement 1 (b) placement 2 (c) placement 3

Fig. 11. The tags' placement of MPT prototype.

V_d^c. If yes, we set $R = 1$. We consider the internal status of the package has not been changed when $R = 1$. On the contrary, if $R = 0$, we consider there may be changes of the internal status and further physical inspection will be conducted. This method takes the two parts of D into account and works very well in our experiments.

4 Multi-Pair of Tags Case

As aforementioned, we have illustrated how to design Echoscope in a case of one Single-Pair of Tags (SPT). However, the SPT design has some limitations. For example, limited by the weak backscattered energy and finite transmission space of a single pair of passive RFID tags, the internal space of a very large package may not be covered by SPT. Hence we want to explore the possibility of extending SPT to a Multi-Pair of Tags (MPT) system. Compared to SPT, MPT utilizes multiple pairs of tags to cover a larger space, and hence can be used for arbitrary-sized packages. This characteristic can improve the usability and user experience of Echoscope.

However, design MPT is also challenging. We should solve two problems introduced by the usage of multiple pairs of tags, which did not exist in the SPT system: 1) how to place multiple pairs of tags in the package, and 2) how to distinguish multiple pairs of tags from a mixture of signals. We propose two corresponding methods, namely group-based placement and length-based distinguishing.

For the first problem, we employ a group-based method for tag placement. As shown in Fig. 11, we use three kinds of placement of eight tags. Intuitively, the first two types, i.e., Fig. 11a and 11b, are not as practical as the third one. The third placement, in which we pair every two close tags as a group, can cover more package spaces with fewer tags. And each group of tags can be considered as a mini SPT. So we adopt the third placement as the default placement of MPT.

For the second problem, we introduce a length-based extracting method. To eliminate the outside environment noises N_{en}, we tend to subtract the signal of one tag from that of another tag in a same group, i.e., $S_1^g - S_2^g$, where g is the index of group. To achieve this goal, we should figure out which two tags are in a group. Here we employ a length-based method. For the tags in a group, we set their EPCs different to each other. For different groups, we use different lengths of EPC, i.e., in different numbers of bits. Specifically, the number of bits of EPC c_{g+1} of the $(g+1)$-th group, is larger (or smaller, we take the larger case as an example) than that of the g-th one, i.e., c_g. In fact, if we set $c_{g+1} \geq 2 \cdot c_g$, the EPC segment signal length L_{g+1} of the $(g+1)$-th group is certainly larger than that of the g-th one, i.e., L_g. By utilizing this observation, we can ensure that the gaps between two groups are certainly larger than that of the tags in a same group. We further illustrate it as follows:

Illustration. If $c_{g+1} \geq 2 \cdot c_g$, the EPC segment signal length L_{g+1} of the $(g+1)$th group is certainly larger than that of the g-th, i.e., L_g.

According to EPC C1G2 protocol [1], tags shall encode the backscattered data via either FM0 based band or Miller modulation. The signal length ℓ of data 0 and 1 are the same. However, due to the different hardware characteristics, the backscatter link frequency varies among tags. In other words, ℓ is different for different tags. We assume the varied range of ℓ is $[a, b]$. In general, the relationship between a and b can be safely assumed as $a < b < 2 \cdot a$. Considering other parameters, such as the encoded mode parameter M_e and modulation mode parameter M_m, the signal length of g th and $g+1$ th group can be expressed as follows:

$$\begin{cases} L_g = M_m \cdot M_e \cdot \ell_g \cdot c_g \\ L_{g+1} = M_m \cdot M_e \cdot \ell_{g+1} \cdot c_{g+1}, \end{cases} \tag{10}$$

where ℓ_g and ℓ_{g+1} represent the larger data length of two tags in group g and $g+1$, respectively. Imaging a most special case that $\ell_g = b$ and $\ell_{g+1} = a$. Under this circumstance, L_g reaches its maximum value while L_{g+1} is minimum. Equation (10) can be transformed to:

$$\begin{cases} L_g = M_m \cdot M_e \cdot b \cdot c_g \\ L_{g+1} = M_m \cdot M_e \cdot a \cdot c_{g+1}. \end{cases} \tag{11}$$

Because a and b hold a relationship of $a < b < 2 \cdot a$, we can draw a conclusion that if we set $c_{g+1} \geq 2 \cdot c_g$, the relationship between L_{g+1} and L_g will be $L_{g+1} > L_g$. In this way, we can distinguish different groups apart by utilizing k-means classification.

To confirm this, we conduct an experiment, in which the monitor uses MPT to collect the EPC segments of 4 pairs of tags and every pair of tags forms one group, i.e., tag 1 and 2, tag 3 and 4, tag 5 and 6, tag 7 and 8. For the tags in a group, we set their EPC codes different to each other. For different groups, we use different length of EPC code, i.e., different number of bits. Specifically, we define the relationship between c_{g+1} and c_g as follows:

$$c_{g+1} = \alpha \cdot c_g + \beta. \tag{12}$$

We alter the values of both α and β. The k-means results are shown in Fig. 12. As Fig. 12a shows, if the EPC bits are all the same for different groups, we can separate each tag apart clearly. However, it is hard to distinguish the groups with each other. For the other three cases, we can easily observe differences between different groups. And the larger the difference between the values of c_{g+1} and c_g, the larger the difference between their k-means results. We employ the last one in MPT, i.e., $c_{g+1} = 2 \cdot c_g$, which demonstrates the best discrimination.

Interestingly, we find that each pair of tags in a single group can be regarded as a SPT system. So we reuse the processing procedure mentioned in Section 3. After the feature extraction, we have a series of trend vectors $\Gamma_t = \{V_t^1, V_t^2, V_t^3, ...V_t^g, ...V_t^G\}$ and detail matrix $\Gamma_d = \{V_d^1, V_d^2, V_d^3, ...V_d^g, ...V_d^G\}$, where G is the total number of tag pairs. We record the trend vector set Γ_t and detail matrix set Γ_d of both check-in and testing cases, and make the final matching decision by using the authentication logic described in last section. Therefore, we get a set of values $\Re = \{R_1^1, R_1^2, R_1^3, ...R_1^g, ...R_1^G\}$ of the

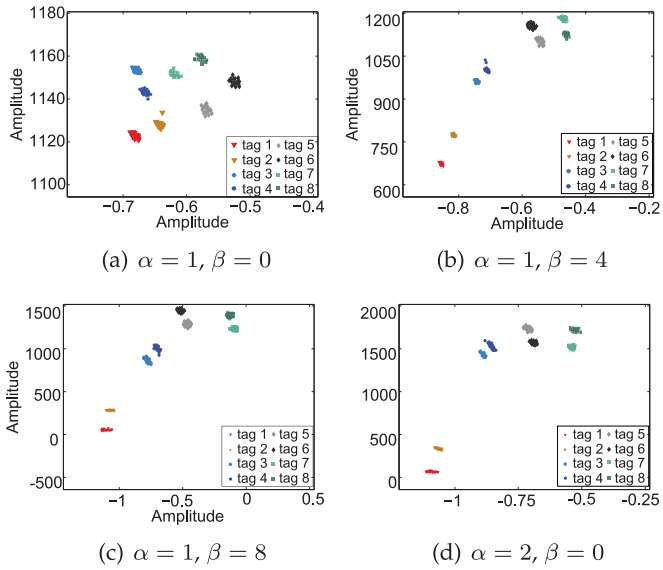

(a) $\alpha = 1, \beta = 0$ (b) $\alpha = 1, \beta = 4$

(c) $\alpha = 1, \beta = 8$ (d) $\alpha = 2, \beta = 0$

Fig. 12. K-means results of different bits of c_{g+1} and c_g.

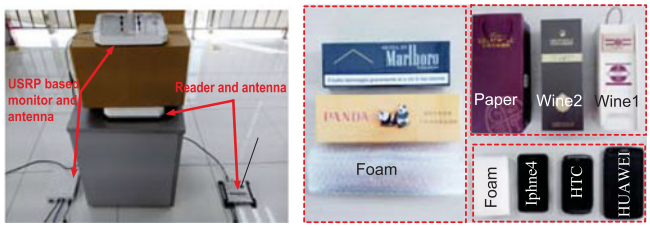

(a) Devices (b) Part of items

Fig. 13. Experimental devices and filling materials.

checking results. We will discuss the result set $\Re$ by varying the threshold $T_{\Re}$ in Section. 5.6.

5 Implementation and Experimental Evaluation

We implement Echoscope using COTS devices and conduct experiments in practical environments to evaluate its performance.

5.1 Prototype System

An Echoscope prototype built with COTS devices is shown in Fig. 13a. It consists of a commercial RFID reader model Impinj R220, a generic USRP monitor, and many tags. We use a USRP N210 plus an SBX daughterboard as the monitor. To show that Echoscope is ubiquitously applicable, we use three mainstream types of tags on the market, i.e., Impinj E41C, Impinj H47 and Alien 964X. In the experiments, we attach two tags of a same type onto the bottom of each package, with the distance of 4 cm in-between. Antennas (Laird S9028PCL) used by both the reader and monitor are circularly polarized with a gain of 8 dBi. We use eight kinds of material to fill the internal space of the packages, including alloy, cloth, carton, glass, paper, plastic, water, and wood. Some of them are shown in Fig. 13b.

5.2 Methodology

All experiments were conducted in the indoor environment where extensive RF noise exists, including WiFi, AM/FM, and Bluetooth signals. We use *different rooms in different buildings* to simulate the check-in and testing sites. We use three different sizes of cardboard packages as the containers. The three sizes are 17 cm $\times$ 19 cm $\times$ 29 cm (denoted as "Small"), 23 cm $\times$ 24 cm $\times$ 40 cm ("Medium"), and 29 cm$\times$ 37 cm$\times$ 52 cm ("Large"). Note that all packages are *arbitrarily* selected and bought online. We did not determine their sizes on purpose.

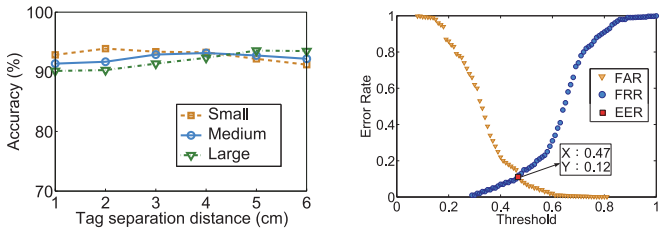

(a) Tag distance vs. accuracy (b) Threshold vs. error rates

Fig. 14. Impact of package size, tag distance, and threshold.

For each set of experiments, we fill each package with one type of material and plastic foam for the remaining space. Items inside the package are arranged orderly and closed to each other without wrapped in other packing materials. In order to simulate the practice, we fill the package until all the items inside cannot move around more than 3 cm under violent shaking. Note that the packing way is also a kind of characteristic of the package, which may be helpful to identify the packages. The experiments are conducted in two phases, check-in and testing. In the check-in phase, Echoscope collects a *record* and computes the reference features for each package. And in the testing phase, we repeat the above steps and compare the features with that in check-in phase.

To evaluate our system, we utilize three suitable metrics, i.e. *accuracy*, *FAR* and *FRR*. In an experiment, if the objects in a package have not been changed and Echoscope reports `accept`$(R = 1)$, or the objects are changed and Echoscope reports `reject`$(R = 0)$, we consider this experiment is successful. The *accuracy* of Echoscope is defined as the ratio of successful ones among all experiments. Besides the accuracy, we also evaluate the false accept rate (*FAR*) and false reject rate (*FRR*) of Echoscope. The *FAR* is the ratio of unsuccessful ones among all experiments that report `accept`. *FRR* is the ratio of unsuccessful ones among all experiments that report `reject`. Obviously, the administrator of logistics systems may have more concerns on FAR than FRR, because false rejects can be avoided using extra testing methods which could be destructive. It is natural that if we suspect the items in a package are changed, we will eventually open the package to check. Hence under the same accuracy, we prefer lower FAR.

5.3 Impact of Package Size, Tag Distance, and Threshold

We discuss the influences of the package size and distance between the two tags. We make use of 5 types of materials (alloy, water, book, clothes, and plastic) and put them into the three sizes of packages. We put the tag pair with a distance from 1 cm to 6 cm and illustrate the accuracy in Fig. 14a and Table 1. We find that the accuracy is always higher than 90 percent and FAR and FRR are mostly under 10 percent. According to the experiment results, it is recommended that for large packages the tag pair should have a distance of $5 \sim 6$ cm. And for the small packages, the distance should be

TABLE 1
Tag Distance versus FAR and FRR

package	results	1 cm∼ 2 cm	3 cm∼ 4 cm	5 cm∼ 6 cm
Small	FAR	5.55%	6.67%	9.22%
	FRR	6.91%	6.70%	8.35%
Medium	FAR	6.11%	6.67%	10.00%
	FRR	7.82%	7.06%	6.93%
Large	FAR	16.67%	8.22%	4.44%
	FRR	8.07%	7.93%	7.00%

$2 \sim 4$ cm. In fact, for tags that with less separate distances will inductive with each other, which may influence the performance of Echoscope. In the next experiments, we utilize the package of the medium size with tags separated by 4 cm.

By comparing the features, the threshold T in identification determines if Echoscope will accept or reject a package. We show the FAR, FRR, and EER (Equal Error Rate, happened when FAR equal to FRR) by varying T in Fig. 14b. Depending on different applications, Echoscope may select a proper T. For example, if we want to maximize the accuracy, we may choose $T = 0.47$ at the point of EER. If we want to have a smaller FRR, T should be smaller than 0.4.

5.4 Impact of Environmental Changes and Moving Objects

We conduct the experiments in both static and dynamic scenarios. In the static scenario we use a same Echoscope prototype (including the RFID reader and monitor) for both the check-in and testing phases. In the dynamic scenario we use different devices for check-in and testing. The static scenario simulates the inventory application in warehouses, and the dynamic scenario simulates the logistics applications across different transit stations. Note that to simulate a real logistic process, we always move the packages and shake them for several seconds before testing. In addition, we also introduce some *human impact*. We allow a volunteer walking around during the dynamic experiments. The region of his movement is from 20 cm to 4 m away from the package. The average moving speed is about 1.5 m/s.

We show the accuracy of Echoscope in Fig. 16a and the FAR and FRR in Fig. 16b for three tag models and three scenarios: static, dynamic, and human impact. We fix the threshold for all experiments. We find that the accuracy is always higher than 90 percent in all cases. The FARs are smaller than 10 percent and FRRs are smaller than 5 percent using a fixed threshold. Among the three models of tags, we find that the Impinj H47 tags have the least FRRs (1.8 to 3.8 percent for three scenarios) and the FARs are as low as those of Alien tags (4.8 to 7.1 percent). In other words, only 4.8 to 7.9 percent packages whose internal objects are changed may not be detected by Echoscope. Echoscope is very robust to dynamic environments and noise introduced by surrounding moving objects.

5.5 Robust to Various Practical Factors

We also conduct experiments to investigate the potential impacts of a number of practical factors.

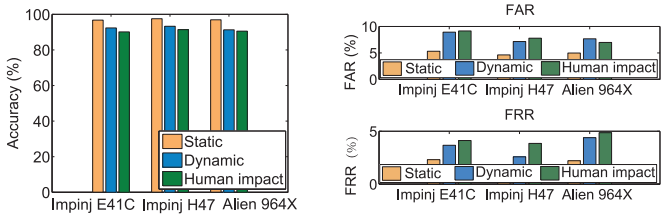

(a) Accuracy (b) FAR and FRR

Fig. 15. Impact of dynamic environments and moving objects.

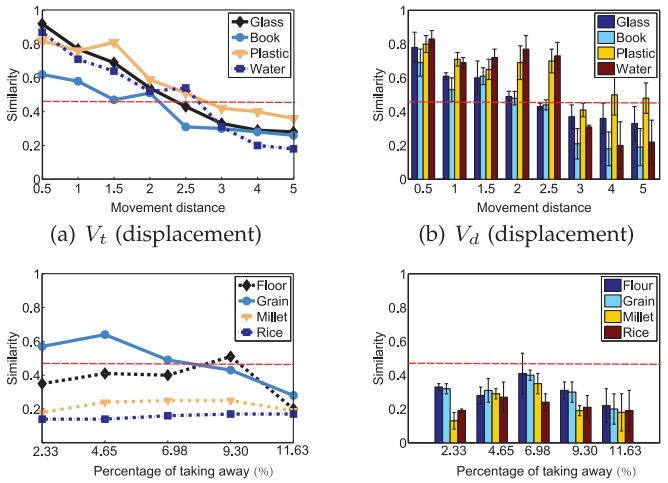

(a) V_t (displacement) (b) V_d (displacement)

(c) V_t (partial removal) (d) V_d (partial removal)

Fig. 16. The average correlation coefficients after displacement or partial removal.

5.5.1 *Sensitivity to Displacement*

Note that in this work Echoscope deals with tightly filled and packed packages. Hence normal logistic operations (such as shaking and vibration) will only yield a small displacement, mostly less than 1 cm. On the other side, abnormal internal changes can easily cause a relatively big displacement. Here we evaluate the sensitivity of Echoscope to the displacement of internal objects.

We use items with four types of material: paper, plastic, bottled water, and glass. For each experiment, we use one of five levels of displacement by changing the object positions from 1 cm to 5 cm. We investigate the cross-correlation coefficients of V_t and V_d respectively between the features of the check-in and testing phases, as the similarities. In this experiments, we set the threshold as $T = 0.47$ (the red lines). Here we use the threshold that selected in Fig. 14b. Note that this threshold is set with the presence of displacement. If one of the similarities V_t and V_d is below the threshold, Echoscope will reject this package. We show in Fig. 16a and 16b the cross-correlation coefficients of V_t and V_d for all materials as well as the threshold (in red lines). When the displacement is within 1 cm, Echoscope will accept all packages. When the displacement is larger than 3 cm, Echoscope will reject all packages. According to life experience, a displacement larger than 3 cm would be obvious in packages. Therefore in practice normal logistic operations will not cause the package to be rejected. In addition, large displacement will be aware to Echoscope. Note that abnormal object changes will not just cause displacement and we will show more results of them.

TABLE 2
The Experiment Result of Similar Objects

Material	Accuracy	FRR	FAR
Phone	94.11%	2.87%	8.56%
Cigarette	98.76%	2.06%	3.54%
Wine	97.89%	1.77%	4.51%

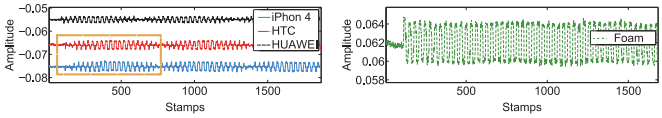

(a) The features of iPhone 4, htc and HUAWEI (b) The features of the foam

Fig. 17. Feature c_a of different types of items after DWT.

Fig. 18. Detect different liquids.

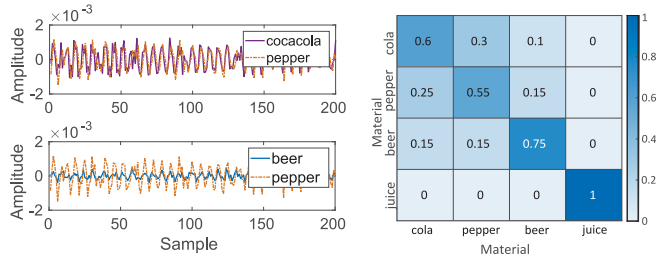

(a) The features of different drinks (b) Confusion matrix

Fig. 19. Different types of drinks

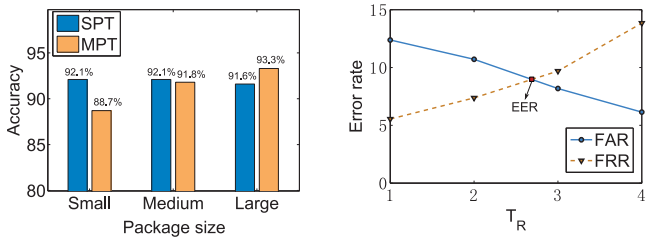

(a) Accuracy vs. SPT (b) Error rate vs. threshold T_R

Fig. 20. The performance of MPT prototype.

5.5.2 Sensitivity to Partial Removal or Substitution

Attackers may take a part of items in a package, instead of taking all items away. We exam the ability of Echoscope to detect such partial removal or substitution.

We fill a medium size package with one of the four kinds of goods, i.e., flour, grain, millet, and rice. We record the features in the check-in phase and then take away a part of them before performing testing. The similarities (in cross-correlation coefficients) of check-in and testing features are shown in Fig. 16c and 16d. The results show that, even only 2.33 percent taking-off will be recognized by Echoscope and the package will be rejected.

We observe similar results for partial substitution. Thus, Echoscope is very sensitive to partial removal and substitution.

5.5.3 Sensitivity to Different Items with Same Material

We now consider another status change of a package. An attacker may substitute the original items with items made in same material, for example, replacing the original wines by much cheaper ones. We conduct our experiments using three types of items (as shown in Fig. 13b), including smart phones, wines, and cigarettes. For each type of items, we replace the original items with another brand (not exactly in the same weight and shape as the original one) and test whether Echoscope can correctly report these changes. The results are shown in Table 2. The most important metric is the FAR that quantifies the false-acceptances by Echoscope after substitution. For the wines and cigarettes, the FAR is very low (4.51 and 3.54 percent respectively). The FAR is higher for smart phones, but Echoscope can still detect most package changes.

We conduct an experiment with three cellphones, i.e., iPhone 4, HTC S510e and HUAWEI G7, and a foam. The foam and HTC have the same shape with iPhone 4. And the HUAWEI is the same weight with iPhone 4. We depict the C_a vector of these four items after performing DWT in Fig. 17. We find that the C_a vectors are quite different among HUAWEI, foam plastics and iPhone 4. However, it is a little difficult to distinguish iPhone 4 and HTC. The C_a vectors are similar for these two items. Thus Echoscope can find out the things with different shapes and materials easily. As a comparison, X-ray cannot distinguish iPhone 4 from the foam, the weighting method cannot tell the difference between HUAWEI and iPhone, and the seal tag method cannot distinguish all of these substitutes.

5.5.4 Sensitivity to Different Types of Liquid

We also conduct an experiment to detect the performance of Echoscope on telling different types of liquid. As shown in Fig. 19, we choose four types of drinks, namely Coca-Cola, Dr. Pepper, beer, and orange juice. The first three drinks have similar type of cans, while the last one is in a plastic bottle. We first fill the package with one type of drink, and extract its features. Then we fill the same package with another type of drink that with the same placement. The features of these liquid are shown as Fig. 18a. We find that Coca-Cola has extremely similar features with those of Dr. Pepper. While though the cans are the same, we can also distinguish pepper and beer. The confusion matrix are shown in Fig. 18b. We find that Echoscope can accurately tell beer, juice from Coca-Cola and Dr. Pepper. However, Coca-Cola and Dr. Pepper are too similar to distinguish.

5.6 Performances of MPT Prototype

We also build a prototype of MPT and conduct evaluation for its performance. The MPT prototype composes of 4 pairs of tags. Note that the number of tag pairs can be increased or decreased on demand. In particular, we compare SPT with MPT on the aspects of package size, to show the effectiveness of MPT. In addition, we decide the appropriate parameters by finding out the Equal Error Rate (EER) point.

We conducted a set of experiments over three different sizes of packages, namely 'Small', 'Medium' and 'Large', with the similar settings in Section 5.2. We still choose the nine types of materials as the content in the package.

The distance between two tags in a same group is 2 cm. The results are shown in Fig. 20a. We find that MPT outperforms SPT only in the large-package case, in which the multiple pairs of tags are not influenced by each other. As a result, we should choose the appropriate number of pairs for different sized packages in practice.

We determine the threshold $T_{\Re}$ by finding out the Equal Error Rate point. We analyze the collected data of the 9 types of materials in the 'Large' package at the check-in and testing cases, respectively. For each pair of check-in and testing data, we obtain a result set $\Re_{m_1}^{m_2}$, where m_1 and m_2 represent the labels of two compared material of check-in and testing cases. Intuitively, if m_1 is the same as m_2, we can make a conclusion that the package had not been replaced or substituted. Since there are G predict results R_g ($g = 1, 2, ..G$) of the G groups of tags (in our experiments, $G = 4$) in the result set $\Re_{m_1}^{m_2}$, we define a threshold $T_{\Re}$ ($0 \leq T_{\Re} \leq G$). If more than $T_{\Re}$ predict results R_g agree with a judgment that the package has not been changed, Echoscope will consider the package as a non-changed one. We alter the value of threshold $T_{\Re}$. The False Accept Rate (FAR) and False Reject Rate (FRR) are shown in Fig. 20b. Theoretically, the interaction point of FAR and FRR is the Equal Error Rate. In Fig. 20b, it is about 9 percent. Then the threshold $T_{\Re}$ is close to 3 (when $G = 4$). Since $T_{\Re}$ should be an integer, we set 3 as its value in this deployment. In this way, we can set different threshold $T_{\Re}$ according to the customer's demands in practice.

6 Discussion

6.1 Comparison to Other Approaches

X-ray Screening. X-ray screening is a widely used method to graphically reveal the internal details of a package. It can retrieve accurate graph of the inner objects and easy to verify. However, the X-ray screening method has several drawbacks. First, it needs extra expensive devices. An X-ray screening machine is about \$30K dollars, which is much costly than RFID devices (about \$2K dollars). Second, the X-ray screening method may incur privacy concerns because the images will reveal the explicit information of the internal items. Third, attackers can cheat the screening-based method by simply replacing with items with same shapes. Compared with RF-based method, the image-based features of x-raying are very easy to predict and simulate. In addition, a tiny displacement of items may introduce huge changes on the x-ray scanning figures. Hence although x-ray screening method is good at detecting structure of inner items for security checks, it is not suitable for package identification.

Ultrasonic testing. Ultrasonic is a non-destructive testing technique based on the propagation of ultrasonic waves in the object or material tested. It is always used in internal flaws detection or material characterization. However, ultrasonic testing is not a good choice in package verification. First, the requirement on extra hardware (about $\$15K$ dollars) and manual process limits the deployment in real practice. In addition, it is too sensitive to tolerate the package changes during the transportation. Some tiny displacement or deformation may introduce large differences on ultrasonic testing. So it is not suitable for package identification applications.

Seal tag. A simple solution is to put a seal tag onto the package, which can not be opened without breaking the seal tag. However, this approach still only verifies the seal tag rather than the internal objects. In practice, it is possible that an attacker uses physical approaches to cheat the testing system. For example, an attacker may open the package and use a forged seal tag with the same ID or bar-code to repack the package.

Weighing. Another simple idea is to weigh the package at all testing locations to find any difference in weight. Though being cost-efficient, this method can be easily cheated by replacing original items with cheap weighting material.

Radar. Radar is an object-detection system that uses radio waves to determine the range, angle, or velocity of objects. But it has many limitations when applying into package identification system. First, it can not reflect complex internal structures of a package. In addition, radar-based approach is also based on the item's shape, which is very easy to simulate.

Echoscope. Echoscope is a non-destructive approach that utilizing the penetration of RF signals. Compared with aforementioned methods, it has several advantages. First, it verifies the inner objects rather than the label on the package. In addition, RF-based features are relevant to multiple characteristics of the inner items, including shape, material, placement, etc.. Since the permittivity of a package is determined by all these aspects mentioned above, only simulating parts of these characteristics would not work to pass the verification by Echoscope. Third, utilizing the deployed RFID systems as the identification system is very economical and reasonable. In fact, there is no 'perfect' solutions that can provide 100 percent security guarantee. RF-based method proposed in Echoscope considers more characteristics of a package. Compared to aforementioned mechanisms, Echoscope makes an attacker much harder to cheat the verification system.

6.2 Impact of Environmental Factors

Signal Penetrability. Echoscope can work in the presence of signal blocking due to the material of internal items. Even if the signal is blocked, it is still diffracted and refracted around the internal items. Such diffraction and refraction can also enable the feature extraction and matching to our approach. For items with strong blocking effect on the RF signal, we suggest to increase the transmission power or employ the tags with better backscattering capacity, e.g., anti-metal tags. In addition Echoscope can employ multiple pairs of tags that pasted on each side of the package. With this deployment, we can always receive diffraction or even refraction signals that penetrate the package.

Container Materials. We choose paper-based boxes in the experiments because most containers in real-world logistic and storage are made by paper. On the other hand, we did evaluate the performance of Echoscope in detecting contents with common materials, such as wood, glass, plastics, and alloy. We found that the RF signals is able to penetrate these materials and distinguish them. Since the container can be considered as a part of the item, the results imply that the material of containers has negligible influence to our system.

Significant Displacement. Echoscope will fail when the items have significant displacement or deformation. Echoscope will be applied to tightly filled and packed packages to verify their internal status. It is useful for applications that use fully filled packages. If the package is not fully

filled, the users could be asked to pack their packages well to guarantee a good identification performance.

The Motion Interference. Echoscope can cope with the motion interference. Assume that a package is moving along a conveyor. The monitor and reader are placed statically on the conveyor. The motion of package will bring two changes, namely the outside environment change and the penetration signal change. The outside environment can be reduced with our mechanism introduced in Section 3.2. In addition, the penetration signal change is introduced by the difference of the penetration paths through the package, which is not frequent during movement over a conveyor. Assume all sites use a same type of conveyors, we can record a series of features when the package is moving. Then at the testing site, we also collect the features when the package is moving with the same speed. In this way, Echoscope can be applied in a moving case.

7 Related Work

A number of technologies have potentials to be the alternatives of Echoscope, including radar, thermography and WiFi. Over all, our approach is much cost-efficient than those techniques. This is because our method reuses the RFID infrastructure, which has been widely deployed in transportation, warehouse, and other logistics-alike applications. From this perspective, implementing our approach will not suffer from purchasing costly hardware, modifying existing application structure, or raising rigid constraints to the deployment. Specifically, Radar is an object-detection system that uses radio waves to determine the range, angle, or velocity of objects [8], [9], [10]. The basic idea behinds radar is transmitting radio waves or microwaves that reflect from any object in their path. However, it requires much more complex and bulky devices and is subject to licensing and regulations (due to larger frequency bandwidth). Thermography uses infrared spectroscopy [11] to achieve high resolution on the produced images. However it is also imagery based. Besides the privacy concern, it has the limitations in the high expense of the larger pixel array and low interpretation accuracy upon erratic temperatures. WiFi based object recognition is also a potential solution but not practical for the application of this work. It is because the diversity of WiFi devices, such as APs and wireless NICs, introduces significant errors to the features extracted from the signals. Meanwhile, current WiFi systems employ a competition based mechanism to allocate the channel resource, inevitably incurring co-channel interferences. In addition, multipath effect is also a challenging issue in indoor environments. Hence, significant errors may be introduced to the feature extraction and matching if using WiFi signal to detect the internal state of objects.

Trustworthy and low-cost RFID have been studied for various applications and platforms [12]. Among these works, Danev et al., [13] focus on identifying HF tags using physical-layer information. Methods proposed in [14], [15], [16] are physical-layer identification for UHF tags. The authors in [15] provide a Minimum Power Response feature extraction method to distinguish different tags, which is the first work on feature extraction of RFID UHF tags. GenePrint [17] presents a physical layer identification method, which utilizes transmitter-specific features introduced by hardware imperfections during manufacturing process of tags. These approaches all focus on identifying tags, because it is generally assumed that tracking tags is equal to tracking the objects they attach to.

Recently, a growing number of studies start to investigate the identification and tracking of real objects or human beings, rather than their tags. In the areas of RF-based sensing, a lot of research projects have been conducted on detection of human motion or static metallic objects, such as those in [18], [19], [20]. Specifically, [18], [19] provide methods that utilize 500 MHz to 3 GHz wideband transmissions to detect human motion and image metallic objects. However, these works rely on expensive and specialized devices, which may limit their widespread uses. A number of systems are proposed to leverage wireless signals to detect and sense human actions such as running, moving and human gesture [21], [22], [5] In particular, solutions for object localization using RFID tags have been proposed [4], [3], [23], [24]. Yang et al. utilize COTS RFID devices to implement centimetre-level localization of passive tag [21]. OTrack is a solution to track a series of tags [25]. The methods proposed in [22] and [5] take advantage of Wi-Fi signals in common rooms to detect human motions and gestures. In particular, Wi-Vi [5] achieves human tracking using statistical angle-of arrival techniques such as MUSIC. Differ from Wi-Vi, Tadar [26] aims to exactly recover object's trajectory using COTS RFID devices. In addition, some other works, such as [27], [28], [29], [30], utilized wireless signals to track or sense the human motion and actions. However, none of them is designed for nondestructive testing.

Except for aforementioned works, a series of alternative technologies, e.g., radar, infrared radiation and WiFi, seem to be suitable for detecting inner changes. Among them, radar is an object-detection system that uses radio waves to determine the range, angle, or velocity of objects [8]. The basic idea behinds radar is transmitting radio waves or microwaves that reflect from any object in their path [9], [10]. However, it can only detect a surface characteristic of the object, which is not suitable for detecting inner changes. And infrared radiation is used in industrial, scientific, and medical applications. Infrared spectroscopy examines absorption and transmission of photons in the infrared energy range [11]. However, infrared method is also based on image. In addition, infrared method is too fine-grained to detect centimeter-level changes in our applications. Finally, it is impractical for WiFi to detect nondestructive testing. Because it is hard to deal with the environment noises and hardware characteristics, which may introduce errors in feature extraction and comparison.

8 Conclusion

We design and implement the first nondestructive package testing and verification system using COTS RFID devices, called Echoscope. We successfully demonstrate that analysis on backscatter signals may reveal internal status of packages, by both theoretical modelling and experimental results. The

evaluation results based on prototyping in practical environments show that Echoscope has very high accuracy to detect abnormal intern changes and low false accept rate. Echoscope works well for a large variety of materials, in both static and dynamic environments with surrounding moving objects.

Acknowledgments

This work was supported by National Basic Research Program of China (973 Program) under Grant No 2015CB351705, NSFC Grant No. 61572396, 61772413, 61672424, and National Science and Technology Major Project of the Ministry of Science and Technology of China JZ- 20150910. Chen Qian was partially supported by National Science Foundation Grants CNS-1717948 and CNS-1750704.

References

[1] EPC Global, EPC radio-frequency identity protocols class-1 generation-2 UHF RFID protocol for communications at 860 MHz–960 MHz," *Version*, vol. 1, p. 23, 2008.
[2] G. Grimmett and D. Stirzaker, Probability and Random Processes. London,London, U.K.: Oxford Univ. Press, 1982.
[3] J. Wang and D. Katabi, "Dude, where's my card?: RFID positioning that works with multipath and non-line of sight," in *Proc. ACM SIGCOMM*, 2013, pp. 51–62.
[4] L. M. Ni, Y. Liu, Y. C. Lau, and A. P. Patil, "LANDMARC: indoor location sensing using active RFID," *Wireless Netw.*, vol. 10, no. 6, pp. 701–710, 2004.
[5] Y. Zheng and M. Li, "Open RFID lab," 2013, [Online]. Available: http://pdcc.ntu.edu.sg/wands/ORL
[6] J. Ou, M. Li, and Y. Zheng, "Come and be served: Parallel decoding for COTS RFID tags," in *Proc. Proc. 21st Annu. Int. Conf. Mobile Comput. Netw.*, 2015, pp. 500–511.
[7] R. D. Wallen, "The illustrated wavelet transform handbook," *Biomed. Instrum. & Tech.*, vol. 38, no. 4, p. 298, 2004.
[8] M. I. Skolnik, "Introduction to radar," in *Radar Handbook*, vol. 2, 1962.
[9] F. E. Nathanson, J. P. Reilly, and M. N. Cohen, "Radar design principles-signal processing and the environment," *NASA STI/Recon Technical Report A*, vol. 91, 1991.
[10] P. Bahl and V. N. Padmanabhan, "RADAR: An in-building RF-based user location and tracking system," in *Proc. IEEE INFOCOM*, 2000, pp. 775–784.
[11] B. Stuart, *Infrared Spectroscopy*. Hoboken, NJ, USA: Wiley Online Library, 2005.
[12] V. Brik, S. Banerjee, M. Gruteser, and S. Oh, "Wireless device identification with radiometric signatures," in *Proc. Proc 14th ACM Int. Conf. Mobile Comput. Netw.*, 2008, pp. 116–127.
[13] B. Danev, S. Capkun, R. Jayaram Masti, and T. S. Benjamin, "Towards practical identification of HF RFID devices," *ACM Trans. Inf. Syst.Secur.*, vol. 15, no. 2, Jul. 2012, Art. on. 7.
[14] D. Zanetti, B. Danev, et al., "Physical-layer identification of UHF RFID tags," in *Proc. 16th Annu. Int. Conf. Mobile Comput. Netw.*, 2010, pp. 353–364.
[15] S. C. G. Periaswamy, D. R. Thompson, and J. Di, "Fingerprinting RFID tags," *IEEE Trans. Dependable Secure Comput.*, vol. 8, no. 6, pp. 938–943, Nov.-Dec. 2011.
[16] Y. Zheng and M. Li, "P-mti: Physical-layer missing tag identification via compressive sensing," in *Proc. IEEE INFOCOM*, 2013, pp. 917–925.
[17] J. Han, C. Qian, P. Yang, D. Ma, Z. Jiang, W. Xi, and J. Zhao, "GenePrint: Generic and accurate physical-layer identification for UHF RFID tags," *IEEE Trans. Netw.*, vol. 24, no. 2, pp. 846–858, 2016.
[18] T. S. Ralston, G. L. Charvat, and J. E. Peabody, "Real-time through-wall imaging using an ultrawideband Multiple-Input Multiple-Output (MIMO) phased array radar system," in *Proc. IEEE Int. Symp. Phased Array Syst. Technol.*, 2010, pp. 551–558.
[19] Y. Wang, M. J. Kuhn, and A. E. Fathy, "Advanced system level simulation of UWB three-dimensional through-wall imaging radar for performance limitation prediction," in *Proc. IEEE MTT-S Int. Microwave Symp.*, 2010, pp. 165–168.
[20] F. Zhu, S. Gao, A. T. S. Ho, T. W. Brown, J. Li, and J.-D. Xu, "Low-profile directional ultra-wideband antenna for see-through-wall imaging applications," *Progress Electromagnetics Res.*, vol. 121, pp. 121–139, 2011.
[21] L. Yang, Y. Chen, X. Li, C. Xiao, M. Li, and Y. Liu, "Tagoram: Real-time tracking of mobile RFID tags to high precision using COTS devices," in *Proc. Proc. 20th Annu. Int. Conf. Mobile Comput. Netw.*, 2014, pp. 237–248.
[22] Q. Pu, S. Gupta, S. Gollakota, and S. Patel, "Whole-home gesture recognition using wireless signals," in *Proc. 19th Annu. Int. Conf. Mobile Comput. Netw.*, 2013, pp. 27–39.
[23] J. Wang, D. Vasisht, and D. Katabi, "RF-IDraw: Virtual touch screen in the air using RF signals," in *Proc. ACM Workshop MOBICOM*, 2014, pp. 235–246.
[24] T. Liu, L. Yang, Q. Lin, Y. Guo, and Y. Liu, "Anchor-free backscatter positioning for RFID tags with high accuracy," in *Proc. IEEE Conf. Comput. Commun.*, 2014, pp. 379–887.
[25] L. Shangguan, Z. Yang, A. X. Liu, Z. Zhou, and Y. Liu, "Relative localization of RFID tags using spatial-temporal phase profiling," in *Proc. 12th USENIX Conf. Netw. Syst. Des. Implementation*, 2015, pp. 251–263.
[26] L. Yang, Q. Lin, X. Li, T. Liu, and Y. Liu, "See through walls with COTS RFID system!" in *Proc. 21st Annu. Int. Conf. Mobile Comput. Netw.*, 2015, pp. 487–499.
[27] H. Ding, L. Shangguan, Z. Yang, J. Han, Z. Zhou, P. Yang, W. Xi, and J. Zhao, "FEMO: A platform for free-weight exercise monitoring with RFIDs," in *Proc. ACM SenSys*, 2015, pp. 141–154.
[28] H. Ding, J. Han, A. X. Liu, J. Zhao, P. Yang, W. Xi, and Z. Jiang, "Human object estimation via backscattered radio frequency signal," in *IEEE Conf. Comput. Commun. (INFOCOM)*, 2015, pp. 1652–1660.
[29] J. Han, H. Ding, C. Qian, D. Ma, W. Xi, Z. Wang, Z. Jiang, and L. Shangguan, "CBID: A customer behavior identification system using passive tags," in *Proc IEEE 22nd Int. Conf. Netw. Protocols*, 2014, pp. 47–58.
[30] F. Adib, Z. Kabelac, and D. Katabi, "Multi-person motion tracking via RF body reflections," in *Proc. 12th USENIX Conf. Netw. Syst. Des. Implementation*, 2015, pp. 279–292.

Ge Wang received the BS degree from Xi'an Technological University, in 2013. She is now working toward the PhD degree at Xi'an Jiaotong University. She is currently a visiting student with the University of California, Santa Cruz. Her research interests include wireless sensor network, RFID, and mobile computing. She is a member of the IEEE.

Jinsong Han received the PhD degree in computer science from Hong Kong University of Science and Technology, in 2007. He is now a professor with Zhejiang University. His research interests include mobile computing, RFID, and wireless network. He is a senior member of the ACM and IEEE.

Chen Qian received the PhD degree from the University of Texas at Austin, in 2013. He is now an assistant professor with the Department of Computer Engineering, University of California Santa Cruz. His research interests include computer networking, data-center networks, software-defined networking, and mobile computing. He is a member of the IEEE and ACM.

Wei Xi received the PhD degree in computer science computer science and technology from Xi'an Jiaotong University, in 2014. He is now an associate professor with Xi'an Jiaotong University. His research interests include wireless networks, smart sensing, and mobile computing. He is a member of the CCF, ACM, and IEEE.

Han Ding received the PhD degree in computer science and technology from Xi'an Jiaotong University, in 2017. She is currently an assistant professor with Xi'an Jiaotong University. Her research interests include RFID system and smart sensing. She is a member of the IEEE.

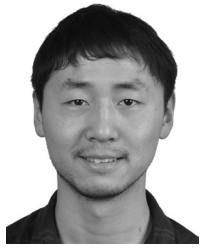

Zhiping Jiang is currently an assistant professor with Xidian University. His research interests include localization, smart sensing, wireless communication, and image processing. He is a member of the IEEE.

Jizhong Zhao received the PhD degree in computer science computer science and technology from Xi'an Jiaotong University, in 2001. His research interests include computer software, pervasive computing, distributed systems, network security. He is a member of the CCF, ACM, and IEEE.